Land–Ocean Warming Contrast over a Wide Range of Climates: Convective Quasi-Equilibrium Theory and Idealized Simulations

MICHAEL P. BYRNE AND PAUL A. O'GORMAN

Massachusetts Institute of Technology, Cambridge, Massachusetts

(Manuscript received 10 May 2012, in final form 28 November 2012)

ABSTRACT

Surface temperatures increase at a greater rate over land than ocean in simulations and observations of global warming. It has previously been proposed that this land–ocean warming contrast is related to different changes in lapse rates over land and ocean because of limited moisture availability over land. A simple theory of the land–ocean warming contrast is developed here in which lapse rates are determined by an assumption of convective quasi-equilibrium. The theory predicts that the difference between land and ocean temperatures increases monotonically as the climate warms or as the land becomes more arid. However, the ratio of differential warming over land and ocean varies nonmonotonically with temperature for constant relative humidities and reaches a maximum at roughly 290 K.

The theory is applied to simulations with an idealized general circulation model in which the continental configuration and climate are varied systematically. The simulated warming contrast is confined to latitudes below 50° when climate is varied by changes in longwave optical thickness. The warming contrast depends on land aridity and is larger for zonal land bands than for continents with finite zonal extent. A land–ocean temperature contrast may be induced at higher latitudes by enforcing an arid land surface, but its magnitude is relatively small. The warming contrast is generally well described by the theory, although inclusion of a land–ocean albedo contrast causes the theory to overestimate the land temperatures. Extensions of the theory are discussed to include the effect of large-scale eddies on the extratropical thermal stratification and to account for warming contrasts in both surface air and surface skin temperatures.

1. Introduction

A robust feature of simulations and observations of global warming is that land surface temperatures increase to a greater extent than ocean surface temperatures (e.g., Manabe et al. 1991; Sutton et al. 2007). This land–ocean surface warming contrast is not predominantly a transient effect due to the different thermal inertias of the land and ocean regions; rather, it appears to be a fundamental response of the climate system to global warming that persists in the equilibrium response of the system. In addition to the importance of the land–ocean warming contrast for societal impacts of climate change, it may also be expected to play a dynamical role by influencing features of the general circulation such as stationary waves.

Several previous studies have investigated the land–ocean warming contrast in fully coupled general circulation model (GCM) simulations (e.g., Sutton et al. 2007; Lambert and Chiang 2007; Fasullo 2010; Boer 2011). The contrast is often characterized in terms of an amplification factor $A \equiv \Delta T_L/\Delta T_O$, where Δ indicates a change between two climates and T_L and T_O are the surface air temperatures over land and ocean, respectively. Using 20 models from the World Climate Research Programme's Coupled Model Intercomparison Project phase 3 (WCRP CMIP3) (Meehl et al. 2007), Sutton et al. (2007) found that the amplification factor based on global-mean surface air temperature varies from 1.36 to 1.84 depending on the model, with a multimodel mean of 1.55. The amplification factor also varies with latitude, with a local minimum of ~1.2 in the tropics and a maximum of ~1.6 in the subtropics in the multimodel mean. The amplification factor remains approximately constant as the radiative forcing increases, but it is somewhat smaller in equilibrium simulations with a ''slab'' ocean (multimodel mean of 1.33) compared

Corresponding author address: Michael Byrne, Massachusetts Institute of Technology (54-1815), 77 Massachusetts Ave., Cambridge, MA 02139-4307.
E-mail: byrnem@mit.edu

DOI: 10.1175/JCLI-D-12-00262.1

with transient simulations with a coupled atmosphere–ocean model (multimodel mean of 1.55).

Analysis of a variety of coupled and uncoupled GCM simulations shows that the land–ocean warming contrast is present in interannual variability and suggests that the interaction between ocean and land is asymmetric, causing the land surface temperature to be more sensitive to the ocean surface temperature than the ocean surface temperature is to the land surface temperature (Compo and Sardeshmukh 2008; Dommenget 2009) [although the degree of asymmetry is not generally agreed upon (Lambert et al. 2011)]. It has been further argued that the majority of land warming in response to anthropogenic forcing is actually forced indirectly by the warming ocean and not by local radiative forcing (Dommenget 2009).

The land–ocean surface warming contrast is also evident in the observational record of recent decades (Sutton et al. 2007; Lambert and Chiang 2007; Drost et al. 2011). The amplification factors derived from observations and models have similar latitudinal structures and comparable low-latitude (40°S–40°N) magnitudes (Sutton et al. 2007). However, agreement between observations and models, and indeed between the models themselves, is poor in the middle to high latitudes of the Northern Hemisphere, which may be partly related to the disparate ice and land surface parameterizations and aerosol forcings employed by the various models.

Differences in the surface energy budget over land and ocean have been invoked to account for the existence of an equilibrium warming contrast (e.g., Manabe et al. 1991; Sutton et al. 2007). Assume, for example, that a surface radiative forcing is applied with equal magnitude over land and ocean. Because of less surface moisture availability over land, cooling by dry-sensible and longwave-radiative fluxes represents a greater portion of the increase in surface cooling required to balance the energy budget, implying a land–ocean contrast in changes in surface air temperature and air–surface temperature disequilibrium (the difference between surface air and surface skin temperature). This simple argument suggests that the land–ocean warming contrast should be larger for drier land regions, as is found to some extent in simulations and observations, although changes in aridity and low cloud cover are also important, even in moist regions (Joshi et al. 2008; Doutriaux-Boucher et al. 2009; Fasullo 2010). Lambert and Chiang (2007) extend the energy approach by including a land–ocean heat flux, which helps to maintain the relatively constant amplification factor that is a feature of observations and simulations (Huntingford and Cox 2000; Sutton et al. 2007). Although these arguments provide an intuitive understanding of why one might expect a land–ocean warming contrast to exist, the surface energy budget alone is not sufficient to give a quantitative estimate of the warming contrast: even if changes in surface relative humidity, soil moisture, and downwelling radiative fluxes are taken as given, the surface energy budget still depends on changes in air–surface temperature disequilibrium in addition to the changes in surface temperature that we wish to estimate.

Rather than attempting to relate land–ocean temperature differences to local energy budgets, Joshi et al. (2008) argue that atmospheric processes provide a strong constraint on the land–ocean warming contrast. Tropospheric lapse rates behave differently over land and ocean because of limited moisture availability over land. If a level exists in the atmosphere at which there is no warming contrast (or no temperature contrast in our version of the theory), then different changes in lapse rates over land and ocean imply different changes in surface air temperature. Furthermore, the constraint from atmospheric processes may apply over a range of time scales, and local radiative forcing over land is not required to obtain an amplification factor greater than unity. This approach is attractive in that it does not involve surface energy fluxes explicitly (which depend on several factors in addition to surface temperature), but it does require an understanding of tropospheric lapse rates in different regimes.

Our study differs from previous studies by investigating the land–ocean warming contrast over a wide range of climates and by comparing theory with simulations from an idealized GCM using a variety of land configurations. The land configurations chosen provide control, ocean-only hemispheres that facilitate a straightforward comparison of land and ocean temperatures (with the exception of simulations with a meridional land band, in which induced stationary waves make interpretations more difficult). Our idealized simulations permit a systematic evaluation of the response of land–ocean temperature contrasts to radiative forcing; such a systematic evaluation is more difficult to accomplish with a full-complexity GCM in which ocean circulations, topography, ice and snow coverage, fixed continents, and other factors make interpretations more troublesome.

We begin by developing a simple theory to estimate the magnitude of the warming contrast (section 2). The theory is based on the hypothesis of Joshi et al. (2008) that the contrast arises from different lapse rates over land and ocean, owing to differences in moisture availability, although we make somewhat different assumptions from Joshi et al. (2008) regarding how the lapse rates are set. We then explore how the warming contrast varies with latitude and with land configuration in a range of simulations with the idealized GCM (section 3).

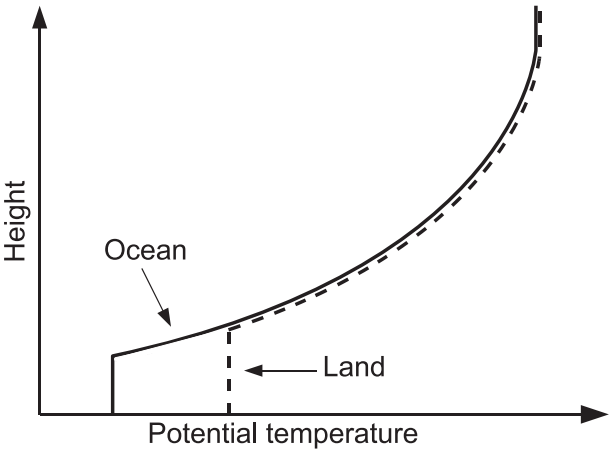

FIG. 1. Schematic diagram of potential temperature vs height for moist adiabats over land and ocean and equal temperatures at upper levels. A land–ocean surface air temperature contrast is implied by different LCLs over land and ocean.

Climate is varied in the idealized GCM by prescribing changes in longwave absorber as a representation of changes in greenhouse gas concentrations or by prescribing different evaporative fractions to directly test the effects of land aridity. Results from the simulations are presented for subtropical (section 4) and higher-latitude (section 5) land surfaces. Extensions of the theory to account for the effect of eddies on the extratropical stratification are discussed (section 5b). The sensitivities of the land–ocean warming contrast to water vapor radiative feedbacks and land–ocean albedo contrasts are assessed with additional sets of simulations (section 6). In all cases, the simulation results are compared to the simple theory. Differences between warming contrasts as measured by surface air temperatures and surface skin temperatures are also described (section 7). The paper concludes with a summary and a brief discussion of outstanding questions (section 8).

2. Theory

We introduce a simple theory that allows for the estimation of the land–ocean surface air temperature difference and warming contrast based on the ocean surface air temperature T_O and the surface relative humidities over ocean and land, $\mathcal{H}_O$ and $\mathcal{H}_L$, respectively. We are motivated by the hypothesis of Joshi et al. (2008) that the land–ocean contrast is constrained by different changes in lapse rates over land and ocean caused by differences in surface moisture availability.

Joshi et al. (2008) make the assumption that the land–ocean warming contrast vanishes sufficiently high in the atmosphere. We make the stronger assumption that the land and ocean temperatures (rather than their changes) are equal sufficiently high in the atmosphere. This assumption simplifies the analysis and should be approximately valid in the tropics because of weak temperature gradients in the tropical free troposphere (e.g., Sobel and Bretherton 2000). Idealized GCM simulations discussed later suggest that the assumption of equal land and ocean temperatures aloft may also be adequate in some cases in the extratropics.

Our second assumption is that lapse rates are moist adiabatic in the mean over land and ocean. By moist adiabatic lapse rates, we mean dry adiabatic lapse rates below the lifted condensation level (LCL) and saturated moist adiabatic lapse rates above it, such that a parcel lifted from near the surface is neutrally buoyant with respect to the mean state of the atmosphere.[1] This assumption implies that our theory is appropriate to the tropics and falls into the class of theories based on convective quasi-equilibrium (e.g., Arakawa and Schubert 1974; Emanuel 2007). In our application of convective quasi-equilibrium, convection is assumed to be sufficiently active so as to maintain moist adiabatic lapse rates in the mean despite large-scale dynamical and radiative forcing.

With these two assumptions, the lapse rates over land and ocean only differ in the vertical range between the LCL over ocean and the LCL over land (Fig. 1). The LCL is higher over land because of lower surface moisture availability. In the vertical range between the LCLs, a saturated moist adiabatic lapse rate Γ_m^* occurs over ocean and a dry adiabat Γ_d occurs over land. Warming results in a reduction in Γ_m^* but leaves Γ_d unchanged. Combined with the assumption of equal temperatures above the LCLs, this implies a greater surface warming over land than ocean. Changes in surface relative humidity affect the LCLs and may also modify the warming contrast. Note that the higher LCL over land implies not only a land–ocean warming contrast, but also a higher surface temperature over land than ocean in the current climate, all else being equal.

Our assumptions allow for the prediction of the land surface air temperature from the ocean surface air temperature and the surface relative humidities over land and ocean. For example, using the air temperature and relative humidity at the ocean surface, we can integrate upward along the moist adiabatic lapse rate from the surface to the level at which the temperature

[1] Joshi et al. (2008) do not assume that mean lapse rates are moist adiabatic over land and ocean in this sense, but instead give an illustrative example in which the lower-tropospheric lapse rate is a weighted average of dry and saturated moist adiabatic lapse rates, with weightings depending on relative humidity.

becomes equal over land and ocean. Using this temperature aloft and the surface relative humidity over land, we can then solve iteratively for the surface air temperature over land (again assuming moist adiabatic lapse rates). In practice, it is simpler to use the equivalent potential temperature θ_e, which we take to be conserved for dry and pseudoadiabatic displacements. The theory amounts to assuming equal surface air θ_e over land and ocean:

$$\theta_e(T_L, \mathcal{H}_L) = \theta_e(T_O, \mathcal{H}_O). \tag{1}$$

Figure 2a shows temperature contrasts for solutions to Eq. (1) for a fixed ocean surface relative humidity of 80% and a range of values of ocean surface air temperature and land surface relative humidity.[2] The temperature contrast is an increasing function of temperature and a decreasing function of surface relative humidity over land; it reaches a value of 25 K for an ocean temperature of 320 K and a land surface relative humidity of 20%.

In the limit of an infinitesimal change in climate, the amplification factor may be written as

$$\begin{aligned} A &= \frac{dT_L}{dT_O} = \frac{\partial T_L}{\partial T_O} + \frac{\partial T_L}{\partial \mathcal{H}_L}\frac{d\mathcal{H}_L}{dT_O} + \frac{\partial T_L}{\partial \mathcal{H}_O}\frac{d\mathcal{H}_O}{dT_O} \\ &= A^T + A^{\mathcal{H}}_L + A^{\mathcal{H}}_O, \end{aligned} \tag{2}$$

where $A^T = \partial T_L/\partial T_O$ is the component of the amplification factor arising from changes in temperature alone, while $A^{\mathcal{H}}_L = (\partial T_L/\partial \mathcal{H}_L)(d\mathcal{H}_L/dT_O)$ and $A^{\mathcal{H}}_O = (\partial T_L/\partial \mathcal{H}_O)(d\mathcal{H}_O/dT_O)$ are the contributions to A due to changes in land and ocean surface relative humidities, respectively. All partial derivatives are calculated assuming equal equivalent potential temperatures over land and ocean according to (1). The amplification factor

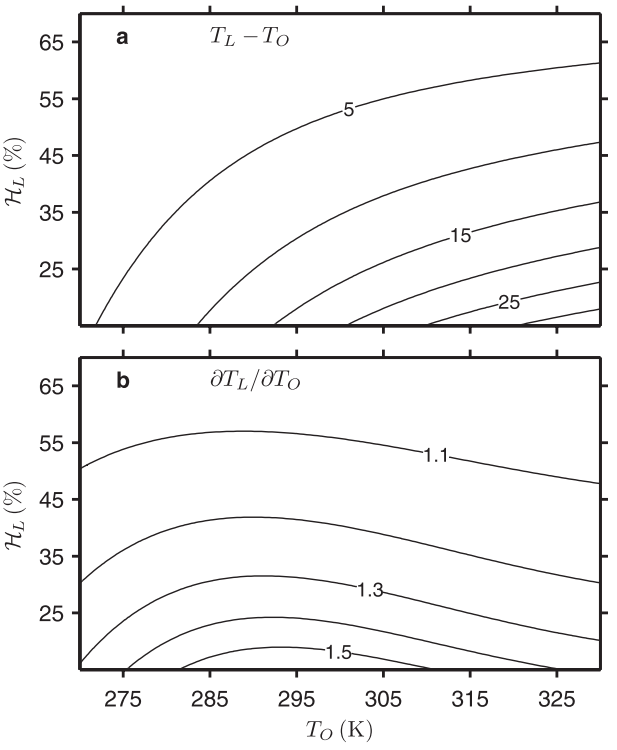

FIG. 2. Theoretical values of (a) the land–ocean surface air temperature difference $T_L - T_O$ (contour interval 5 K) and (b) the amplification factor $A^T = \partial T_L/\partial T_O$ (contour interval 0.1) at constant relative humidities for a range of surface relative humidities over land and temperatures over ocean. Surface relative humidity over ocean is fixed at 80%. The temperature differences and amplification factors are calculated by numerically solving the equal equivalent potential temperature Eq. (1).

at constant relative humidity, A^T, increases monotonically with decreasing relative humidity over land (Fig. 2b). However, the amplification factor varies nonmonotonically with temperature and has a maximum at an ocean surface air temperature of roughly 290 K for the relative humidities considered here. This nonmonotonic behavior arises because, although the saturated moist adiabatic lapse rate is a monotonically decreasing function of temperature, it has an inflection point with respect to temperature at approximately 273 K (calculated at 900 hPa), which gives rise to the peak in the amplification factor. The amplification factor depends on the lapse rates in the layer between the LCLs over land and ocean (cf. Fig. 1), and the temperature of this layer is lower than that of the surface. As a result, the maximum in Fig. 2b occurs at a surface air temperature that is higher than the inflection-point temperature of 273 K.

Changes in surface relative humidity under global warming must also be taken into account; decreases of up to 2% K^{-1} over land were found by O'Gorman and Muller (2010) for a multimodel mean of CMIP3 simulations.

[2] We calculate θ_e using Eq. (9.40) from Holton (2004), with the temperature at the LCL evaluated using Eq. (22) from Bolton (1980). It will later be important that the θ_e used is consistent with the convection scheme in the idealized GCM. We tested this by calculating the land–ocean surface air temperature contrast $T_L - T_O$ implied by (1) using two different means of calculating θ_e: first, using the θ_e formula mentioned above, and second, by lifting a surface air parcel pseudoadiabatically to the top pressure level of the GCM (at which essentially all water has been removed from the parcel) using the saturated moist adiabatic lapse rate that is incorporated in the GCM (Appendix D.2 of Holton 2004) and then returning to the surface along a dry adiabat. For example, based on a land surface relative humidity of 40%, an ocean surface relative humidity of 80%, and an ocean surface air temperature of 290 K, the land–ocean temperature contrast was approximately 6 K and the difference between the two estimates described above was 0.25 K. Thus, we conclude that the formula used for θ_e is adequate for our study.

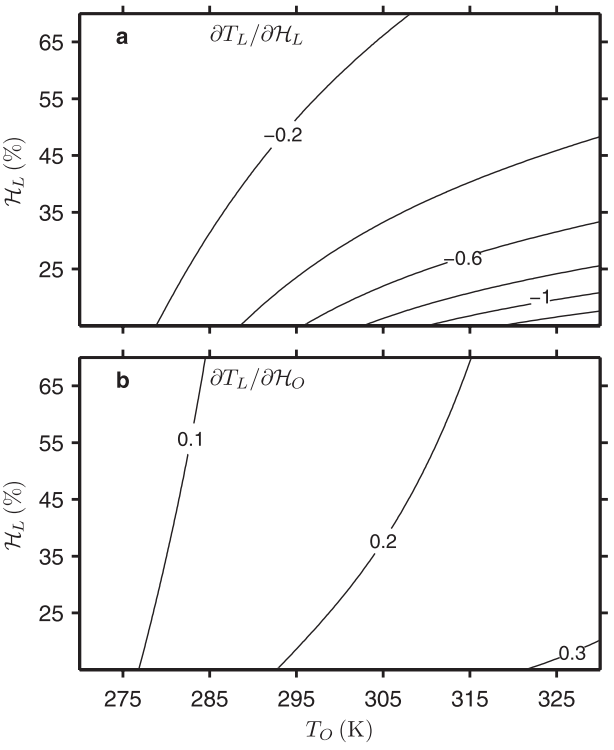

FIG. 3. Theoretical values for the partial derivatives of land surface air temperature with respect to (a) surface relative humidity over land ($\partial T_L/\partial \mathcal{H}_L$) and (b) surface relative humidity over ocean ($\partial T_L/\partial \mathcal{H}_O$) as a function of land relative humidity and ocean temperature [contour interval 0.2 K %$^{-1}$ in (a) and 0.1 K %$^{-1}$ in (b)]. Surface relative humidity over ocean is fixed at 80%. The partial derivatives are calculated by numerically solving the equal equivalent potential temperature Eq. (1).

The change in land surface air temperature for a given change in land surface relative humidity at constant ocean surface air temperature ($\partial T_L/\partial \mathcal{H}_L$) is plotted in Fig. 3a. For an ocean surface air temperature of 295 K and land and ocean surface relative humidities of 50% and 80%, respectively, $\partial T_L/\partial \mathcal{H}_L \approx -0.2$ K %$^{-1}$, and taking $d\mathcal{H}_L/dT_O \approx -2\%$ K^{-1}, we find that $A_L^{\mathcal{H}} \approx 0.4$. This demonstrates that changes in land relative humidity may contribute significantly to the amplification factor according to the theory.

Changes in ocean surface relative humidity in simulations of climate change are generally smaller than changes over land (O'Gorman and Muller 2010) and are thought to be energetically constrained (Schneider et al. 2010). For a typical increase in ocean surface relative humidity of 0.5% K^{-1}, and again taking an ocean surface air temperature of 295 K and land and ocean surface relative humidities of 50% and 80%, respectively, we find that $\partial T_L/\partial \mathcal{H}_O \approx 0.15$ K %$^{-1}$ (Fig. 3b) and $A_O^{\mathcal{H}} \approx 0.08$, which is considerably smaller than the contribution from land relative humidity variations (calculated above as $A_L^{\mathcal{H}} \approx 0.4$).

Given that the theory relies on lapse rates being close to moist adiabatic in the mean, as follows from convective quasi-equilibrium in the convecting regions of the tropics, we refer to it as a convective quasi-equilibrium theory of the surface warming contrast. In the presence of other stabilizing influences on the stratification in addition to convection (such as large-scale eddies in the extratropics) the theory is not strictly applicable, although it may still be a useful guide. The extension of the theory to include the effects of large-scale eddies on the extratropical thermal stratification is discussed in section 5b.

A simple generalization of the theory is possible, also consistent with the concept of convective quasi-equilibrium, in which lapse rates are not assumed to be exactly moist adiabatic, but rather, the departures of lapse rates from moist adiabatic are assumed to remain constant as climate changes. This generalized theory may be formulated by assuming that the surface air equivalent potential temperatures are not necessarily equal over land and ocean, but that their changes are. The land–ocean warming contrast will be higher than for the standard theory if the surface air equivalent potential temperature is higher over ocean than land. The generalized theory does not give more accurate predictions for the idealized simulations presented here, but it may be useful for more realistic simulations or observations.

3. Idealized GCM

a. Land configurations

The idealized GCM has a lower boundary consisting of various configurations of land and a mixed-layer ocean (Fig. 4). Simulations are performed with zonal land bands in the subtropics (20°–40°N) and extratropics (45°–65°N), a continent of finite zonal extent (20°–40°N, 0°–120°E), and a meridional land band (0°–60°E).

b. Model and simulations

We use a moist idealized GCM similar to that of Frierson et al. (2006) and Frierson (2007), with the specific details documented by O'Gorman and Schneider (2008b), except for the introduction of land hydrology (described later in this section) and an alternative radiation scheme that allows for water vapor radiative feedback (described in section 6a). The model is based on a version of the Geophysical Fluid Dynamics Laboratory (GFDL) dynamical core and solves the hydrostatic primitive equations spectrally at T42 resolution with 30 vertical sigma levels. Moist convection is parameterized using a simplified version of the Betts–Miller scheme (Frierson 2007), in which temperatures are relaxed to a moist adiabat and humidities are relaxed to a reference

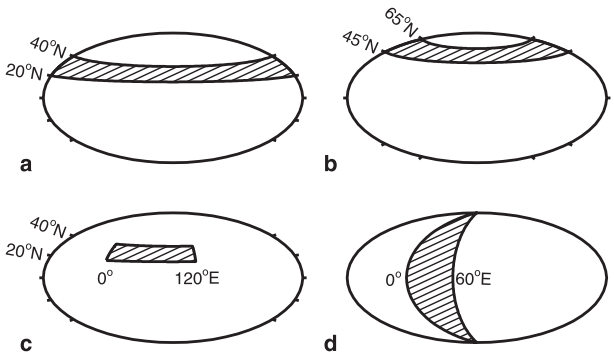

FIG. 4. Simulations are performed using a variety of land configurations: zonal bands (a) from 20° to 40°N and (b) from 45° to 65°N, (c) continent spanning 20°–40°N and 0°–120°E, and (d) meridional band from 0° to 60°E.

profile with a relative humidity of 70%. A large-scale condensation scheme prevents gridbox supersaturation. Reevaporation of precipitation is not permitted, and only the vapor–liquid phase change of water is considered. The top-of-atmosphere insolation is a representation of an annual-mean profile, and there is no diurnal cycle.

Longwave radiative fluxes are calculated using a two-stream gray radiation scheme, and shortwave heating is specified as a function of pressure and latitude. A range of climates is simulated by varying the longwave optical thickness as a representation of the radiative effects of changes in water vapor and other greenhouse gases. In the default radiation scheme, the longwave optical thickness is specified and does not depend explicitly on the water vapor field, excluding all radiative feedbacks of water vapor or clouds. Both longwave and shortwave cloud radiative effects are excluded in the model. The longwave optical thickness is specified by $\tau = \alpha\tau_{\text{ref}}$, where τ_{ref} is a function of latitude and pressure, and the parameter α is varied[3] over the range $0.2 \leq \alpha \leq 6$. The reference value of $\alpha = 1$ corresponds to an Earth-like climate with a global-mean surface air temperature of 288 K for the simulation with a subtropical land band.

Land and ocean surfaces have the same albedo (0.38) and heat capacity (corresponding to a layer of liquid water of depth 1 m and specific heat capacity 3989 J kg^{-1} K^{-1}). The effect of a land–ocean albedo contrast on the warming contrast is explored in section 6b. Horizontal heat transport is not permitted below either surface. Surface fluxes are calculated using bulk aerodynamic formulae and Monin–Obukhov similarity theory, with roughness lengths of 5×10^{-3} m for momentum and 10^{-5} m for moisture and sensible heat over both land and ocean. A k-profile scheme is used to parameterize boundary layer turbulence (Troen and Mahrt 1986).

The simple bucket model of Manabe (1969) is used to simulate the land surface hydrology. The field capacity S_{FC} in the bucket model is the maximum amount of water that can be held per unit area of land surface and has dimensions of depth. Field capacity generally depends on soil type, vegetation, and other factors, but we set $S_{\text{FC}} = 0.15$ m for simplicity (as in Manabe 1969). Soil moisture S also has dimensions of depth and evolves according to

$$\frac{dS}{dt} = \begin{cases} P - E & \text{if} \quad S < S_{\text{FC}} \quad \text{or} \quad P \leq E \\ 0 & \text{if} \quad S = S_{\text{FC}} \quad \text{and} \quad P > E, \end{cases}$$

where P and E are the precipitation and evaporation rates, respectively. Accordingly, soil moisture accumulates when precipitation exceeds evaporation until the field capacity is reached, at which point any subsequent excess of precipitation over evaporation is assumed to run off. Evaporation over land is given by $E_L = \beta E_0$, where β is the evaporative fraction and E_0 is the potential evaporation rate (the evaporation rate obtained over a saturated land surface using bulk aerodynamic formulae). The evaporative fraction β is specified as a linear function of soil moisture up to an upper bound of 1:

$$\beta = \begin{cases} 1 & \text{if} \quad S \geq \gamma S_{\text{FC}} \\ S/(\gamma S_{\text{FC}}) & \text{if} \quad S < \gamma S_{\text{FC}}, \end{cases}$$

where $\gamma = 0.75$. This definition ensures that the soil moisture cannot become negative and that the potential evaporation rate is reached before soil moisture reaches the field capacity. Although the bucket model ignores complexities such as canopy cover and stomatal effects [see Seneviratne et al. (2010) for a review of soil moisture–climate interactions], it is adequate for the purposes of exploring the effect of limited surface moisture availability on the response of surface air temperatures and atmospheric lapse rates to changes in radiative forcing.

Simulations are generally spun up from an isothermal rest state over 3000 days for $\alpha < 1$ and 1000 days for $\alpha \geq 1$, with the exception of the simulations with a midlatitude zonal land band and prescribed evaporative fractions (1500 days) and the simulations with a meridional land band (3000 days). Longer spin-up times are required in colder climates because specific humidities and water vapor fluxes are smaller in magnitude, with the result that soil moisture values take longer to reach statistical equilibrium.

[3] There are nine simulations for each of the subtropical and midlatitude zonal land bands and the subtropical continent (α values of 0.2, 0.4, 0.7, 1.0, 1.5, 2.0, 3.0, 4.0, and 6.0).

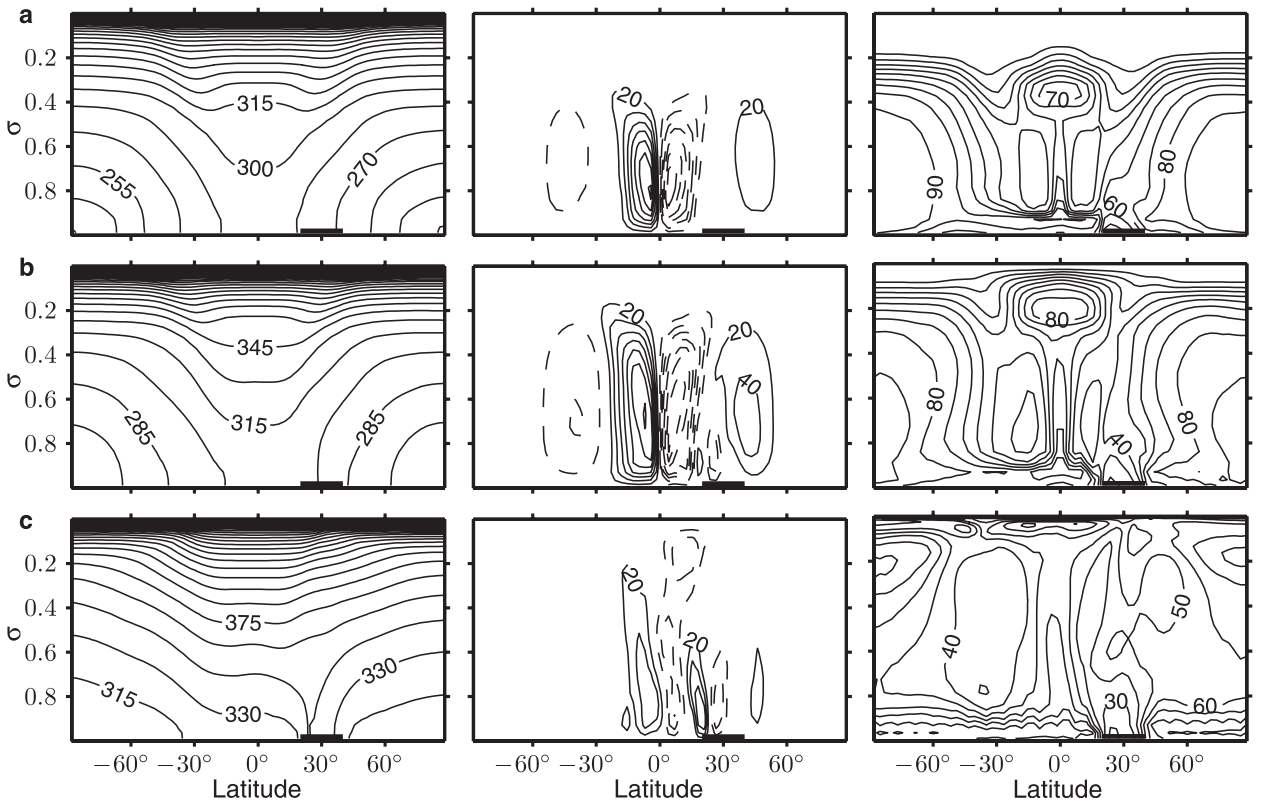

FIG. 5. (left) The zonal- and time-mean potential temperature (contour interval 15 K), (middle) Eulerian-mean streamfunction (contour interval 20×10^9 kg s^{-1}, with negative values given by dashed contours), and (right) relative humidity (contour interval 10%) for a zonal land band from 20° to 40°N in (a) a cold simulation ($\alpha = 0.4$), (b) the reference simulation ($\alpha = 1$), and (c) the warmest simulation ($\alpha = 6$). The heavy black bars indicate the position of the subtropical zonal land band (20°–40°N).

Time averages are taken over the 500-day period after spinup (or over the 1000 days after spinup in the case of the simulations with a midlatitude zonal band and prescribed evaporative fraction and those with a meridional land band). Similar results are generally found using a 200-day average. For example, differences between the land–ocean temperature contrast for the 200- and 500-day averages are less than 0.3 K for the subtropical land band simulations.

c. *Zonal-mean climatology (subtropical zonal land band)*

Figure 5 shows the mean potential temperature, meridional streamfunction, and relative humidity for three simulations ($\alpha = 0.4$, 1, and 6) with a subtropical zonal land band from 20° to 40°N. In the cold simulation ($\alpha = 0.4$), the land does not have a strong influence on the atmospheric state beyond a moderate decrease in the low-level relative humidity over the land band. The reduction in relative humidity is greater in the reference simulation ($\alpha = 1$), and it is a dominant feature in the warm simulation ($\alpha = 6$), in which it extends upward from the surface to $\sigma \simeq 0.5$, where σ is pressure normalized by surface pressure. The enhanced warming over land affects the near-surface temperature structure by weakening the meridional temperature gradient equatorward of the land band and strengthening the gradient on the poleward side in the reference simulation; it causes a reversed temperature gradient on the equatorward side of the land band in the warmest simulation. Shallow monsoon circulations are evident in both the reference and warmest simulations. The quasi-equilibrium theory of monsoons associates the upward branch of direct thermal circulations with local boundary layer maxima in either equivalent potential temperature or potential temperature (Emanuel 1995). An observational analysis of the various regional monsoons on Earth by Nie et al. (2010) shows that two distinct circulation types exist: one is a deep and moist circulation (with upward branch near the boundary layer maximum of equivalent potential temperature), and the other is a mixed circulation composed of a shallow dry cell (with upward branch near the boundary layer maximum in potential temperature) superimposed on the deep moist cell. The monsoon circulations in our simulations show some similarities to the

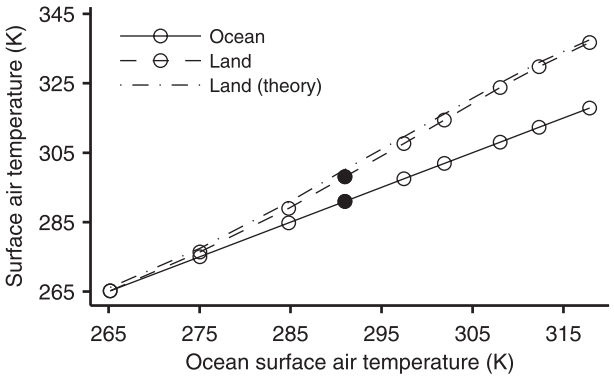

FIG. 6. Surface air temperature over ocean (solid line with circles) and land (dashed line with circles) vs ocean surface air temperature for a subtropical zonal land band from 20° to 40°N. Filled circles denote the reference simulation ($\alpha = 1$) here and in subsequent figures. The dashed–dotted line is the estimate of surface air temperature over land from theory.

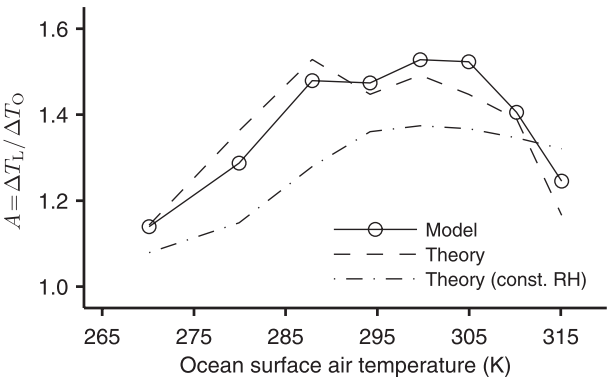

FIG. 7. The amplification factor vs ocean surface air temperature in simulations with a subtropical land band from 20° to 40°N (solid line with circles), from theory (dashed line), and from theory neglecting changes in relative humidity (dashed–dotted line). The amplification factor is calculated based on temperature differences between pairs of nearest-neighbor simulations and is plotted against the midpoint ocean temperature for each pair. The amplification factor from theory is obtained in the same way, but using the theoretical estimates of the land temperature (dashed–dotted line in Fig. 6). The amplification factor from theory neglecting changes in relative humidities [corresponding to A^T in (2)] is evaluated using the surface relative humidities from the colder of the pair of simulations when estimating the land temperature in the warmer simulation.

mixed circulations observed by Nie et al. (2010); the addition of a seasonal cycle to our GCM might lead to a closer resemblance by shifting the boundary layer maximum in equivalent potential temperature poleward in summer. A more detailed study of the changing strength and character of these monsoonal circulations as the climate is varied is left to future work.

4. Subtropical warming contrast

a. Subtropical zonal land band

We first consider simulations with a subtropical zonal land band from 20° to 40°N. The land surface air temperature for a given simulation T_L is defined as the temperature of the lowest atmospheric level ($\sigma = 0.989$) averaged in time and over all land grid points (with area weighting). To make meaningful comparisons of land and ocean regions, we define the ocean surface air temperature to be the average of the lowest-level temperatures over the corresponding region in the other hemisphere. For example, in the case of the zonal land band from 20° to 40°N, the ocean surface air temperature T_O is calculated by averaging over 20°–40°S.

The land–ocean contrast in temperature is close to zero in the coldest climate and increases in magnitude as the climate warms, reaching 19 K in the warmest simulation (Fig. 6). The land–ocean amplification factor has a mean value of 1.4 over all simulations and varies nonmonotonically with ocean temperature (Fig. 7). The mean value is of similar magnitude to the Sutton et al. (2007) low-latitude (40°S–40°N) estimates of 1.51 and 1.54 for climate-model simulations and observations, respectively, although close agreement with our simulations is not necessarily expected given the differences in continental configuration, surface aridity and heat capacity, and radiative forcing.

The estimate of T_L based on theory matches the simulated land temperatures well over the full range of simulations, with an overestimation of T_L of order 1 K in each simulation (dashed–dotted line in Fig. 6). For the theory, the equivalent potential temperatures in Eq. (1) are evaluated using T_O and the surface relative humidities (evaluated at the lowest model level) averaged in time and over land or the corresponding region over ocean. The estimates of the amplification factor from theory are also accurate (dashed line in Fig. 7). There is a maximum in the simulated amplification factor at $T_O \simeq 300$ K, which is higher than the temperature at which the theoretical maximum occurs for constant relative humidities (cf. Fig. 2b), but these should not be directly compared because of changes in the relative humidities in the simulations. In the coldest simulation ($\alpha = 0.2$), the surface relative humidities over land and ocean are 51% and 74%, respectively. Ocean relative humidity remains approximately constant over the full range of climates, but land relative humidity decreases with warming to 24% in the reference simulation ($\alpha = 1$) and remains roughly unchanged over the warmer simulations (not shown). The impact of changes in relative humidity is illustrated by comparison with the theoretical amplification factors assuming unchanged relative humidities (dashed–dotted line in Fig. 7). Not accounting for changes in

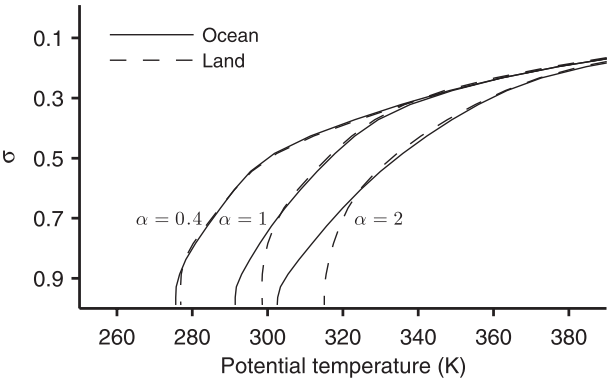

FIG. 8. Vertical profiles of potential temperature averaged in time and over land (dashed) and the corresponding ocean region (solid) for cold, reference, and warm simulations ($\alpha = 0.4$, 1, and 2, respectively) with a subtropical zonal land band from 20° to 40°N.

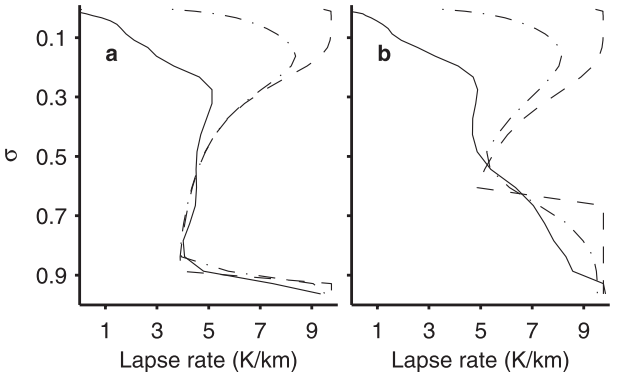

FIG. 9. Vertical profiles of lapse rates averaged in time and over (a) ocean and (b) land for a warm simulation ($\alpha = 2$ and a global-mean surface air temperature of 302 K) with a subtropical zonal land band from 20° to 40°N. The solid lines show the simulated lapse rates, the dashed lines correspond to moist adiabats calculated using the mean surface air temperatures and mean surface relative humidities, and the dashed–dotted lines correspond to averages of moist adiabats weighted according to the PDFs of surface relative humidity following (3). Note that the theory only requires that the lapse rates be moist adiabatic up to the level at which the temperature profiles converge, approximately $\sigma = 0.6$ for this simulation (Fig. 8).

relative humidity results in a substantial underestimation of the amplification factor for all but the warmest two simulations (between which the land relative humidity increases slightly), indicating that the land–ocean surface warming contrast is tightly coupled to changes in low-level relative humidity.

We next examine the accuracy of each of the assumptions made in the theory. The assumption that there is a level at which the land–ocean temperature difference vanishes is found to hold in our simulations (Fig. 8). The fact that this level rises as the climate warms is not an issue since the theory only requires that such a level exists. The assumption of moist adiabatic lapse rates below this level is accurate over ocean, but it is not very accurate over land (Fig. 9), which may be related to moist convection occurring less frequently over the relatively dry land. The vertical temperature profile over land in the GCM simulations is generally more stable than moist adiabatic, and this is consistent with the slight overestimation of the land–ocean surface air temperature contrast by the theory (Fig. 6).

The deviation of the mean thermal stratification from moist adiabatic over land is not as great as might be inferred from comparison with a moist adiabat based on mean surface relative humidity (dashed lines in Fig. 9). We make a second comparison that allows for variability in low-level relative humidity by using estimated probability density functions (PDFs) of surface relative humidity when calculating the moist adiabats. The PDF-weighted moist adiabatic lapse rate $\Gamma_m^{\mathrm{pdf}}(\sigma)$ at a given level σ is computed as

$$\Gamma_m^{\mathrm{pdf}}(\sigma) = \int_0^{100\%} f(\mathcal{H})\Gamma_m(T, \mathcal{H}, \sigma)\, d\mathcal{H}, \qquad (3)$$

where $f(\mathcal{H})$ is the PDF of surface relative humidity and $\Gamma_m(T, \mathcal{H}, \sigma)$ is the lapse rate at σ for a moist adiabat calculated using a surface air temperature of T and a surface relative humidity of $\mathcal{H}$. Figure 9 shows that Γ_m^{pdf} is a somewhat better approximation to the simulated lapse rates over land compared with lapse rates based on moist adiabats calculated using mean surface relative humidities. We make a corresponding estimate of T_L using the PDFs of surface relative humidity over land and ocean rather than the mean values. (We calculate the temperature at the level at which the land–ocean contrast vanishes by integrating Γ_m^{pdf} over ocean from the surface to that level, and we then solve iteratively for T_L using Γ_m^{pdf} over land.) The resulting estimates of T_L are almost indistinguishable from the estimates using mean surface relative humidities (not shown). These results suggest that although variability in surface relative humidity over land results in variability in the LCL and effectively smooths the time-mean lapse rates in the vertical (Fig. 9b), use of mean surface relative humidities is still adequate when applying the equal equivalent potential temperature Eq. (1) to estimate land temperatures.

b. Subtropical continent

The subtropical warming contrast is further investigated using a continent that extends from 20° to 40°N and 0° to 120°E (Fig. 4c). The ocean temperatures are averaged over 20°–40°S and 0°–120°E. The land–ocean

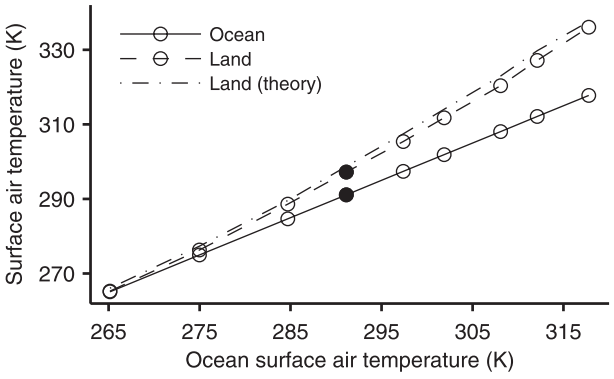

FIG. 10. Surface air temperature over ocean (solid line with circles) and land (dashed line with circles) vs ocean surface air temperature for a land continent spanning 20°–40°N and 0°–120°E. The dashed–dotted line is the estimate of the land temperature from theory.

temperature difference for the continent is smaller than for the corresponding subtropical land band simulations in all but the coldest climate (e.g., it is approximately 2 K smaller for $\alpha = 1.5$ and an ocean temperature of 297 K). The theoretical estimates match the continental land–ocean temperature contrasts, although the land temperatures are slightly overestimated, as for the subtropical band simulations (Fig. 10). The reduced warming contrast compared to the zonal land band is consistent with higher surface relative humidity over the continent (28% over the continent versus 23% over the subtropical band for $\alpha = 1.5$). Higher relative humidity is to be expected over a continent of finite zonal extent because of zonal moisture fluxes from surrounding oceanic regions.

c. *The effect of aridity*

The results above illustrate that limited moisture availability can generate a land–ocean temperature contrast and that this contrast increases as the climate warms in response to radiative forcing. For the simulations discussed so far, the soil moisture and the evaporative fraction have been dynamic quantities that vary in response to changes in the local balance of evaporation and precipitation as the climate warms. To isolate the effect of aridity on the land–ocean temperature contrast, we perform a series of simulations with fixed longwave optical thickness ($\alpha = 1$) and a range of specified values of the evaporative fraction[4] β over a zonal land band from 20° to 40°N. Reducing the evaporative fraction is a simple means of systematically drying out the land surface; it may also be taken as an analog for decreased soil moisture levels in a warmer climate or reduced stomatal conductance and evapotranspiration in elevated CO_2 environments (cf. Joshi and Gregory 2008).

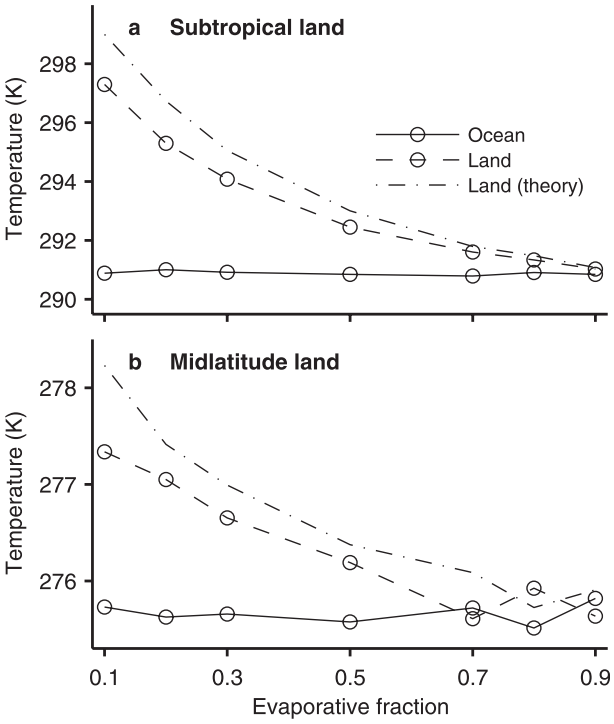

FIG. 11. Surface air temperature over ocean (solid line with circles) and land (dashed line with circles) vs evaporative fraction β for (a) a subtropical zonal land band from 20° to 40°N and (b) a midlatitude zonal land band from 45° to 65°N. The dashed–dotted lines are the estimates of land temperature from theory. The longwave absorber parameter α has its reference value of unity in all simulations.

For $\beta = 1$, land and ocean are identical in the idealized GCM. Reducing β from unity inhibits evaporation from the land surface, and the surface relative humidity over land decreases. According to our theory (Fig. 2), a reduction in relative humidity over land, along with roughly constant relative humidity and temperature over ocean, implies an increase in temperature over land so as to maintain equal equivalent potential temperatures over land and ocean. This behavior is found in our idealized model simulations, with the land–ocean temperature contrast increasing strongly as β is lowered, and doing so roughly in accordance with the theory (Fig. 11a). However, as the land surface relative humidities decrease, the lapse rates depart to a greater degree from moist adiabats, and surface air equivalent potential temperatures over land and ocean diverge, leading to less precise land temperature estimates from the theory. The effect of varying β at midlatitudes is discussed in the next section.

[4] Simulations with β values of 0.1, 0.2, 0.3, 0.5, 0.7, 0.8, and 0.9 are performed for both subtropical (20°–40°N) and midlatitude (45°–65°N) zonal land bands.

5. Higher-latitude warming contrast

By considering a zonal land band at midlatitudes and a meridional land band at all latitudes, we next investigate how the land–ocean warming contrast depends on latitude and whether the theory can account for the magnitude of extratropical warming contrasts.

a. Midlatitude zonal land band

For the midlatitude zonal land band (45°–65°N), there is effectively no land–ocean warming contrast when climate change is forced by varying the longwave absorber over the range $0.2 \leq \alpha \leq 6$ (not shown). Moisture flux convergence is sufficient at these latitudes to maintain soil moisture levels close to, or at, field capacity, and land and ocean surfaces behave similarly.

The lack of a land–ocean warming contrast at midlatitudes is robust and easily understood in the case of our idealized GCM, but simulations with comprehensive GCMs suggest that the land–ocean warming contrast is not confined to lower latitudes (e.g., Sutton et al. 2007). Land surfaces and moisture convergence regimes in Earth's extratropics are more diverse than in our idealized GCM, and relatively arid regions occur there regionally and seasonally [for example, mean surface relative humidity in summer over Mongolia and neighboring parts of Russia is substantially lower than over ocean regions at similar latitudes (Dai 2006)]. Midlatitude soil drying under global warming may occur because of decreased and earlier snowmelts (Rowell and Jones 2006), and such behavior is also not found in our idealized GCM, which has no seasonal cycle or snow or ice.

To examine the effect of limited moisture availability at higher latitudes in the idealized GCM, we prescribe different evaporative fractions in a series of simulations while holding the longwave absorber parameter fixed at $\alpha = 1$ (as for the simulations over a subtropical zonal land band discussed in section 4c). A temperature contrast develops as the evaporative fraction β is reduced, with $T_L - T_O \simeq 1.5$ K for $\beta = 0.1$ (Fig. 11b), although this is substantially smaller than the 6 K difference for the subtropical land band at the same value of β. The theory roughly predicts the magnitude of the temperature contrast and suggests that the reduced temperature contrast relative to lower latitudes is due to both lower temperatures and higher relative humidities further poleward (cf. Fig. 2). According to the theory, these effects are of similar importance in contributing to the reduced land–ocean temperature contrast at higher latitudes.

b. Midlatitude theory

One of the assumptions used in the theory, that the land–ocean temperature contrast vanishes aloft, is found to be adequate in the simulations with a midlatitude land band. But extratropical lapse rates are more stable than moist adiabatic because of the effects of large-scale eddies, and so it is somewhat surprising that the theory based on moist adiabatic lapse rates gives a reasonable estimate of the magnitude of the midlatitude warming contrast. The fact that land–ocean temperature contrasts are sensitive to lower-tropospheric lapse rates (cf. Fig. 1) may be a contributing factor, since simulated extratropical lapse rates are closest to moist adiabatic in the lower troposphere (Schneider and O'Gorman 2008).

There are theories of the extratropical static stability that take account of moisture and large-scale eddies (Juckes 2000; Frierson 2008; Schneider and O'Gorman 2008; O'Gorman 2011). The results of O'Gorman (2011) suggest that the dry static stability may be written as the sum of an effective static stability and a contribution from moisture that is a fraction (roughly 0.6) of the dry static stability along a moist adiabat. If this contribution from moisture is the primary difference in the dry static stability over land and ocean, then the surface warming contrast theory is easily modified for the extratropics by multiplying the predicted warming contrast by roughly a factor of 0.6.

Alternatively, the theory of Juckes (2000) suggests that the vertical gradient in equivalent potential temperature is proportional to the meridional temperature gradient. If this relationship is taken to hold separately over land and ocean, then the predicted surface warming contrast should be unchanged by extratropical eddies if meridional temperature gradients are the same over land and ocean [and similarly for the formulation of Frierson (2008) and Frierson and Davis (2011), but with meridional equivalent potential temperature gradients].

The midlatitude temperature contrasts shown in Fig. 11b are consistent with a modification to the predicted surface warming contrast by an order one factor, but clearly further work is needed to evaluate these theories for the extratropical surface warming contrast.

c. Meridional land band

We examine the land–ocean warming contrast over all latitudes simultaneously using two simulations ($\alpha = 1$ and $\alpha = 1.5$) with a meridional land band from 0° to 60°E in longitude (Fig. 4d). Land temperatures at each latitude are obtained by averaging in time and zonally from 0° to 60°E, while ocean temperatures are averaged in time and zonally from 180° to 240°E. Local minima occur near the equator in both the land–ocean temperature difference (not shown) and the amplification factor (Fig. 12). These equatorial minima coincide with atmospheric moisture flux convergence and relatively high levels of soil moisture. Maxima in the amplification factor occur at ~15° north and south, coincident with

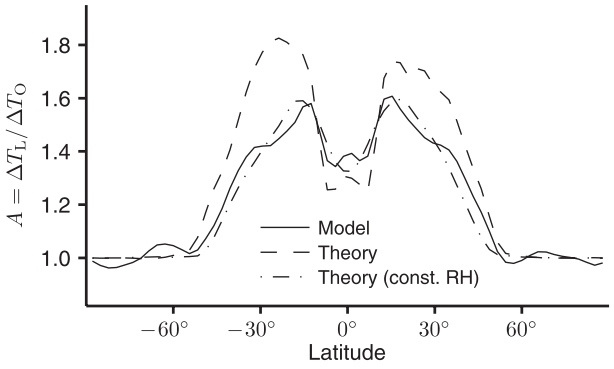

FIG. 12. The amplification factor vs latitude for warming between two simulations ($\alpha = 1$ and $\alpha = 1.5$) with a meridional land band from 0° to 60°E (solid line). The dashed line is the estimate of the amplification factor from theory, and the dashed–dotted line is the estimate from theory neglecting changes in relative humidity. Interhemispheric asymmetry is indicative of sampling error.

the descending branches of the Hadley cells. The land–ocean warming contrast decreases sharply in midlatitudes; according to the theory, this reflects both the poleward increase in relative humidity over land and the poleward decrease in temperature (Fig. 5). The land and ocean temperatures are almost equal poleward of 50° latitude. By comparison, mean precipitation exceeds mean evaporation over ocean poleward of approximately 38° latitude.

The theoretical amplification factors are less accurate for the meridional band simulations than for the subtropical zonal land band or continent, particularly at subtropical latitudes (Fig. 12). The inaccuracy in this case is partly due to deviations from moist adiabatic lapse rates over land, but it may also relate to stationary waves excited by the land band and the lack of an ocean-only Southern Hemisphere to compare with. The amplification factor calculated from theory at constant surface relative humidities seems to be reasonably accurate at all latitudes (Fig. 12), but this results from a compensation of errors. The results from the meridional land band simulations suggest that further work is needed to better quantify the factors affecting the accuracy of the theory and to determine how best to compare land and ocean temperatures in the same hemisphere.

d. Polar amplification

Given the abundance of land at northern high latitudes, it is difficult to cleanly distinguish in observations or comprehensive climate model simulations between polar amplification of temperature changes and land–ocean warming contrast. A number of processes contribute to polar amplification, including ice–albedo feedback, changes in ocean circulation, polar cloud cover, and atmospheric heat transport (Holland and Bitz 2003; Hall 2004; Bony et al. 2006). Although the idealized GCM does not include many of these processes, it still shows a polar amplification effect under climate change (O'Gorman and Schneider 2008a; see also Alexeev et al. 2005). The meridional land band simulations presented here show negligible land–ocean warming contrast beyond 50° latitude (Fig. 12), which implies that the processes involved in establishing a land–ocean temperature contrast at low to midlatitudes are distinct from those responsible for polar amplification in this GCM. We do note, however, that other work suggests radiative feedbacks associated with changing water vapor concentrations may be an important component of both polar amplification and of land–ocean contrasts (Dommenget and Flöter 2011), and land–ocean radiative contrasts are discussed in the next section.

6. Land–ocean radiative contrasts

The simulations so far have included only a land–ocean contrast in surface hydrology. Albedo contrasts or radiative feedbacks from the contrast in humidity could also affect the land–ocean warming contrast, potentially in a manner that is not captured by the theory presented earlier. For instance, decreases in the longwave optical thickness in response to lower evaporative fraction could tend to lower the surface temperature over land (e.g., Molnar and Emanuel 1999) and reduce the land–ocean temperature contrast.

a. Water vapor radiative feedbacks

To assess the effect of longwave radiative feedbacks on the land–ocean temperature contrast, an alternative radiation scheme is used in which the longwave optical thickness depends on humidity according to

$$\frac{d\tau}{d\sigma} = a\mu + bq, \tag{4}$$

where τ is the longwave optical thickness (set to zero at the top of the atmosphere), $a = 0.8678$ and $b = 1997.9$ are nondimensional constants, and q is the specific humidity [this formulation is similar to that of Merlis and Schneider (2010), except that the longwave optical thickness in their study depends on column water vapor rather than specific humidity]. To facilitate comparison between simulations with the different radiation schemes, the values of a and b were chosen by fitting (4) with $\mu = 1$ to the longwave optical thickness averaged from 20° to 40°N for a reference ($\alpha = 1$) aquaplanet simulation with the default radiation scheme. With this choice of

parameters, water vapor is the dominant longwave absorber at all latitudes for the reference value of $\mu = 1$. Atmospheric shortwave heating is prescribed as in the default radiation scheme. Feedbacks associated with shortwave absorption by water vapor are not considered here and may also influence the land–ocean temperature contrast.

For the subtropical zonal land band (20°–40°N), we vary the radiative parameter μ over the range $0.4 \leq \mu \leq 2$ as a representation of the longwave-radiative effect of changes in greenhouse gases other than water vapor.[5] We also consider simulations with specified evaporative fraction β over the range $0.1 \leq \beta \leq 0.9$ and with $\mu = 1$. The results from both sets of simulations are qualitatively similar to those performed using the default radiation scheme (not shown). The land–ocean temperature contrast is slightly higher than for the default radiation scheme (by approximately 2 K for $\alpha = 4$ in the dynamic soil moisture simulations and by approximately 0.5 K at $\beta = 0.5$ in the prescribed evaporative fraction simulations). For the midlatitude zonal land band (45°–65°N), we consider simulations with prescribed evaporative fractions over the same parameter range as for the subtropical land band, and the land–ocean temperature contrasts are found to be roughly the same as in the simulations with the default radiation scheme. For both subtropical and midlatitude land simulations, the theoretical estimates are of similar or better accuracy when compared with the estimates for the simulations with the default radiation scheme.

There are only modest land–ocean temperature differences associated with water vapor radiative contrasts in our simulations. However, the study of Dommenget and Flöter (2011), using a globally resolved energy balance model, suggests a greater role for water vapor radiative feedbacks in setting the land–ocean warming contrast. The idealized nature of the gray radiation scheme used here precludes us from making any definitive conclusions on this issue based on our simulations.

b. Albedo contrast

The importance of land–ocean albedo contrast in determining the land–ocean warming contrast is assessed using a series of simulations in which the ocean surface albedo is set to a smaller value of 0.20 and the land surface albedo remains at 0.38 (the albedo is 0.38 over both land and ocean in our other simulations). Note that cloud albedo effects are not included in the idealized GCM, and the surface albedo values used are not intended to be realistic. The simulations are with a subtropical zonal land band (20°–40°N) and use the default radiation scheme in which the longwave absorber is varied over the range $0.2 \leq \alpha \leq 6$.

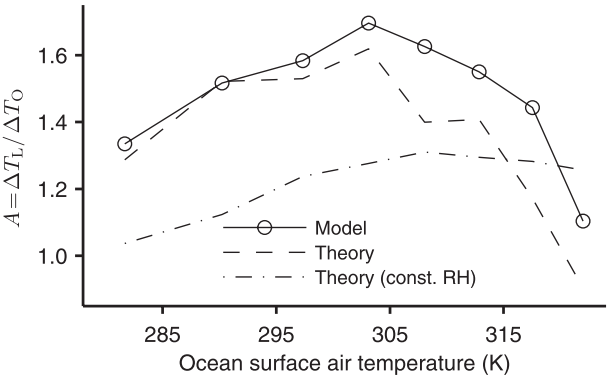

FIG. 13. The amplification factor vs ocean surface air temperature in simulations with a land–ocean albedo contrast and a subtropical zonal land band from 20° to 40°N (solid line). The amplification factors from theory (dashed line) and from theory neglecting changes in relative humidity (dashed–dotted line) are also shown. The ocean albedo is 0.20 and the land albedo has the default value of 0.38. The amplification factors are calculated as in Fig. 7.

The simulated climates are warmer than those presented in section 4a because of the reduced ocean albedo. The land–ocean temperature contrasts are also affected by the albedo contrast, and the land is actually colder than the ocean for the $\alpha = 0.2$ and $\alpha = 0.4$ simulations, despite the lower surface air relative humidity over land. The theory overestimates the land temperatures by as much as 7 K. The amplification factors in these albedo contrast simulations (Fig. 13) are also somewhat larger compared to the simulations presented in section 4a (cf. Fig. 7). However, the theoretical amplification factors are still reasonably accurate, albeit with some underestimation in warm climates.

The overestimation of land temperatures in the simulations with an albedo contrast is primarily related to temperatures over land and ocean not converging aloft. As a result, the generalized theory discussed at the end of section 2, in which lapse rates can deviate from moist adiabatic, is not helpful. (The difference in surface air equivalent potential temperature between land and ocean increases from 12 K in the coldest simulation to 44 K in the warmest simulation.) The assumption made by Joshi et al. (2008) of a fixed land–ocean temperature difference at a certain upper level may be more appropriate here, but modifying the theory to use it would require additional assumptions regarding the choice of upper level. Given that the amplification factors from the theory are reasonably accurate, the simplest approach seems to be to use the theory to estimate the amplification factors, with the understanding that the land temperatures

[5] Simulations are performed with μ values of 0.4, 0.7, 1, 1.5, and 2.

(as opposed to their changes) may be overestimated because of albedo contrast.

7. Surface air versus surface skin temperature

The results discussed so far are for surface air temperatures, but surface skin temperatures may not respond in the same way to climate change. Figure 14 shows that surface skin temperatures are generally larger than surface air temperatures in the subtropical zonal land band simulations (with the default radiation scheme and albedo values). The amplification factors for the surface air and surface skin temperatures are similar, but with somewhat larger amplification factors for surface skin temperatures below $\simeq$305 K, as may be inferred from Fig. 14. For example, for an ocean surface air temperature of 285 K, the amplification factors based on surface skin and surface air temperatures are 1.67 and 1.48, respectively.

The air–surface temperature disequilibrium (the difference between the surface air and surface skin temperatures) decreases as the climate warms and does so more strongly over ocean than over land (Fig. 14). Changes in the air–surface temperature disequilibrium may be understood in terms of the surface energy budget, since the surface energy fluxes (particularly the dry sensible heat flux) are strongly coupled to it. As the climate warms, evaporative cooling of the surface generally increases because of the dependence of the saturation vapor pressure on temperature. The increased evaporative cooling is partially balanced by a reduction in dry sensible cooling, as reflected in the decrease in air–surface temperature disequilibrium, in order to maintain the surface energy balance. Increases in evaporative cooling are smaller over land than ocean and are inhibited by the land becoming increasingly arid, explaining why the air–surface temperature disequilibrium does not decrease to the same extent over land, and why amplification factors are somewhat larger for surface skin temperatures.

The air–surface temperature disequilibrium may be large for very arid land regions in a given climate (e.g., Pierrehumbert 1995), but this does not mean it will necessarily change greatly in these regions as the climate changes (as compared to the land–ocean surface warming contrast). For example, the amplification factors based on surface air and surface skin temperatures are similar in our warm simulations in which the land is very arid. Rather, we may expect these amplification factors to differ most in regions with substantial changes in aridity of the land surface as the climate changes.

As discussed in the introduction, it is difficult to build a theory of the surface warming contrast based solely on the surface energy budget because changes in both the surface temperature and air–surface temperature disequilibrium may play an important role in the adjustment of the surface energy budget over land and ocean. The theory presented in section 2 based on convective quasi-equilibrium gives an independent estimate of the land–ocean warming contrast in surface air temperatures, which may be combined with the constraint of the surface energy budget. As a result, we argue that surface skin warming contrasts may be best understood based on the theory for the surface air warming contrasts and an understanding of changes in the surface energy budget.

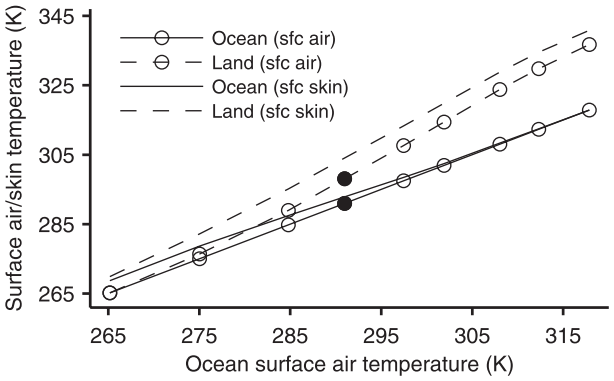

FIG. 14. Surface air temperature over ocean (solid line with circles) and land (dashed line with circles), as well as surface skin temperature of the ocean (solid line) and land (dashed line) vs ocean surface air temperature for simulations with a subtropical zonal land band from 20° to 40°N. The same spatial and temporal averaging is used for the skin temperatures as for the surface air temperatures.

Global observational datasets often provide skin temperatures over ocean (sea surface temperatures) and surface air temperatures over land. For our simulations, the amplification factors using land surface air temperatures and ocean surface skin temperatures are similar to those calculated solely from surface skin temperatures and larger than those calculated solely from surface air temperatures. Since our theory is most appropriate for surface air temperatures, it may underestimate amplification factors calculated from temperature anomalies in these mixed observational datasets.

8. Conclusions

Based on the idea that differential changes in lapse rates over land and ocean constrain the surface warming contrast (Joshi et al. 2008), we have developed a simple theory that relates the land surface air temperature and the land–ocean warming contrast to the ocean temperature and the surface relative humidities over land and ocean. The theory amounts to setting the surface air

equivalent potential temperature to be equal over land and ocean. For constant relative humidities, the theory implies that the amplification factor has a maximum at roughly 290 K for typical relative humidities, a property that follows from the temperature dependence of the saturated moist adiabatic lapse rate. Thus, if two land regions at different latitudes are equally arid, it will be the region whose surface air temperature is closest to 290 K that exhibits the largest warming contrast, according to the theory. Changes in surface relative humidities also play an important role in determining the magnitude of the warming contrast; the theory yields expressions for the additive contributions to the amplification factor from changes in surface relative humidity over land and ocean.

We have applied the theory to simulations with a wide range of climates and land configurations in an idealized GCM. The warming contrast in the equilibrium response of the GCM is primarily confined to low and middle latitudes. For simulations with a subtropical zonal land band forced by changes in longwave optical thickness, the amplification factor is roughly 1.4, which is comparable to low-latitude amplification factors found in observations and simulations with comprehensive GCMs. For a subtropical continent of finite zonal extent, more analogous to what is found on Earth, the magnitude of the land–ocean contrast is reduced compared with the zonal land band as a result of higher relative humidities over the continent compared with the zonal band.

For the subtropical zonal land band and the subtropical continent, the theory closely matches the simulated temperature contrasts over the full range of simulations. It has a similar level of accuracy in an alternative set of simulations in which land aridity is systematically varied by specifying the evaporative fraction. It performs less well when applied to simulations with a meridional land band, although the latitudinal dependence of the warming contrast is still captured.

Atmospheric moisture convergence at middle and high latitudes maintains the soil moisture at close to the field capacity, and there is little warming contrast in the simulations at these latitudes. A midlatitude warming contrast may be induced by directly specifying a low evaporative fraction, and the theory gives a rough estimate of its magnitude. According to the theory, the midlatitude warming contrast is relatively small because of higher relative humidities and lower surface temperatures compared to lower latitudes. The midlatitude stratification is generally more stable than moist adiabatic because of large-scale eddies, implying that the theory is not strictly applicable. We have discussed the extension of the theory to the extratropical regime based on theories of the moist extratropical stratification. The extended theories suggest that the magnitude of the implied warming contrast may be changed by only an order one factor from that given by the convective quasi-equilibrium theory. Further work is needed to evaluate these extended theories for the extratropical warming contrast.

The simulated warming contrast is found to be slightly higher for the subtropical zonal land band when a radiation scheme that allows for water vapor radiative feedbacks is used, and the theory is still adequate for these simulations. But the theory consistently overestimates the land temperatures when the albedo over ocean is set to be lower than over land. The amplification factor from the theory is still reasonably accurate in the presence of the albedo contrast, except in very warm climates.

Overall, the simple theory is successful in capturing the main features of the land–ocean warming contrast resulting from changes in moisture availability and a proxy for greenhouse gases in the idealized GCM simulations. However, deviations of the lapse rates over land from moist adiabatic reduce the accuracy of the theory. This is perhaps not very surprising given that convective quasi-equilibrium should not be expected to hold when, for example, moist convection is infrequent or in large-scale conditions conducive to the formation of inversion layers. Also, the theory is not expected to capture the effect of different changes in albedo over land and ocean, even if it is adequate for estimating the amplification factor for an invariant albedo contrast.

The amplification factors in the simulations are found to be different depending on whether surface air or skin temperatures are considered (or a mixture of the two, as in some observational datasets). Given that the difference between surface air and surface skin temperatures is controlled by the surface energy budget, we argue that an understanding of surface skin warming contrasts for a given level of land aridity follows from a combination of the theory for surface air warming contrasts and the additional constraints of the surface energy balances over land and ocean.

The theory and simulations presented here are expected to be useful in analyzing the factors contributing to land–ocean warming contrasts in observations and in simulations with comprehensive climate models. The theory is likely to be most useful at low latitudes where the effects of moisture availability are strongest and the assumptions underlying the theory are most appropriate. Differences in roughness length, cloud cover, diurnal cycle, and seasonal cycle between land and ocean regions were not accounted for in our idealized simulations; the influence of these factors on the warming contrast could also be examined in an idealized setting. Further work is also needed to examine the sensitivity of our results to the choice of convective parameterization and land surface

scheme. Lastly, as discussed in the introduction, the amplification factor can vary depending on whether transient or equilibrium simulations are considered or if forcing is applied separately over land or ocean, and it would be interesting to examine how this relates to surface humidity changes in light of the theory presented here.

Acknowledgments. We thank Dorian Abbot and Tim Cronin for helpful discussions and Yohai Kaspi for providing an updated postprocessing code. This work was supported in part by the federal, industrial, and foundation sponsors of the MIT Joint Program on the Science and Policy of Global Change and by NSF grant AGS-1148594.

REFERENCES

Alexeev, V. A., P. L. Langen, and J. R. Bates, 2005: Polar amplification of surface warming on an aquaplanet in ''ghost forcing'' experiments without sea ice feedbacks. *Climate Dyn.,* **24,** 655–666.

Arakawa, A., and W. H. Schubert, 1974: Interaction of a cumulus cloud ensemble with the large-scale environment, Part I. *J. Atmos. Sci.,* **31,** 674–701.

Boer, G., 2011: The ratio of land to ocean temperature change under global warming. *Climate Dyn.,* **37,** 2253–2270.

Bolton, D., 1980: The computation of equivalent potential temperature. *Mon. Wea. Rev.,* **108,** 1046–1053.

Bony, S., and Coauthors, 2006: How well do we understand and evaluate climate change feedback processes? *J. Climate,* **19,** 3445–3482.

Compo, G. P., and P. D. Sardeshmukh, 2008: Oceanic influences on recent continental warming. *Climate Dyn.,* **32,** 333–342.

Dai, A., 2006: Recent climatology, variability, and trends in global surface humidity. *J. Climate,* **19,** 3589–3606.

Dommenget, D., 2009: The ocean's role in continental climate variability and change. *J. Climate,* **22,** 4939–4952.

——, and J. Flöter, 2011: Conceptual understanding of climate change with a globally resolved energy balance model. *Climate Dyn.,* **37,** 2143–2165.

Doutriaux-Boucher, M., M. J. Webb, J. M. Gregory, and O. Boucher, 2009: Carbon dioxide induced stomatal closure increases radiative forcing via a rapid reduction in low cloud. *Geophys. Res. Lett.,* **36,** L02703, doi:10.1029/2008GL036273.

Drost, F., D. Karoly, and K. Braganza, 2011: Communicating global climate change using simple indices: An update. *Climate Dyn.,* **39,** 989–999, doi:10.1007/s00382-011-1227-6.

Emanuel, K., 1995: On thermally direct circulations in moist atmospheres. *J. Atmos. Sci.,* **52,** 1529–1536.

——, 2007: Quasi-equilibrium dynamics of the tropical atmosphere. *The Global Circulation of the Atmosphere,* T. Schneider and A. H. Sobel, Eds., Princeton University Press, 186–218.

Fasullo, J. T., 2010: Robust land–ocean contrasts in energy and water cycle feedbacks. *J. Climate,* **23,** 4677–4693.

Frierson, D. M. W., 2007: The dynamics of idealized convection schemes and their effect on the zonally averaged tropical circulation. *J. Atmos. Sci.,* **64,** 1959–1976.

——, 2008: Midlatitude static stability in simple and comprehensive general circulation models. *J. Atmos. Sci.,* **65,** 1049–1062.

——, and N. A. Davis, 2011: The seasonal cycle of midlatitude static stability over land and ocean in global reanalyses. *Geophys. Res. Lett.,* **38,** L13803, doi:10.1029/2011GL047747.

——, I. M. Held, and P. Zurita-Gotor, 2006: A gray-radiation aquaplanet moist GCM. Part I: Static stability and eddy scale. *J. Atmos. Sci.,* **63,** 2548–2566.

Hall, A., 2004: The role of surface albedo feedback in climate. *J. Climate,* **17,** 1550–1568.

Holland, M. M., and C. M. Bitz, 2003: Polar amplification of climate change in coupled models. *Climate Dyn.,* **21,** 221–232.

Holton, J. R., 2004: *An Introduction to Dynamic Meteorology.* 4th ed. Elsevier Academic Press, 535 pp.

Huntingford, C., and P. M. Cox, 2000: An analogue model to derive additional climate change scenarios from existing GCM simulations. *Climate Dyn.,* **16,** 575–586.

Joshi, M. M., and J. M. Gregory, 2008: Dependence of the land-sea contrast in surface climate response on the nature of the forcing. *Geophys. Res. Lett.,* **35,** L24802, doi:10.1029/2008GL036234.

——, ——, M. Webb, D. Sexton, and T. Johns, 2008: Mechanisms for the land/sea warming contrast exhibited by simulations of climate change. *Climate Dyn.,* **30,** 455–465.

Juckes, M. N., 2000: The static stability of the midlatitude troposphere: The relevance of moisture. *J. Atmos. Sci.,* **57,** 3050–3057.

Lambert, F. H., and J. C. H. Chiang, 2007: Control of land-ocean temperature contrast by ocean heat uptake. *Geophys. Res. Lett.,* **34,** L13704, doi:10.1029/2007GL029755.

——, M. J. Webb, and M. M. Joshi, 2011: The relationship between land–ocean surface temperature contrast and radiative forcing. *J. Climate,* **24,** 3239–3256.

Manabe, S., 1969: Climate and the ocean circulation. *Mon. Wea. Rev.,* **97,** 739–774.

——, R. J. Stouffer, M. J. Spelman, and K. Bryan, 1991: Transient responses of a coupled ocean–atmosphere model to gradual changes of atmospheric CO_2. Part I: Annual mean response. *J. Climate,* **4,** 785–818.

Meehl, G. A., C. Covey, T. Delworth, M. Latif, B. McAvaney, J. F. B. Mitchell, R. J. Stouffer, and K. E. Taylor, 2007: The WCRP CMIP3 multi-model dataset: A new era in climate change research. *Bull. Amer. Meteor. Soc.,* **88,** 1383–1394.

Merlis, T. M., and T. Schneider, 2010: Atmospheric dynamics of earth-like tidally locked aquaplanets. *J. Adv. Model. Earth Syst.,* **2,** 17 pp., doi:10.3894/JAMES.2010.2.13.

Molnar, P., and K. A. Emanuel, 1999: Temperature profiles in radiative-convective equilibrium above surfaces at different heights. *J. Geophys. Res.,* **104,** 24 265–24 271.

Nie, J., W. Boos, and Z. Kuang, 2010: Observational evaluation of a convective quasi-equilibrium view of monsoons. *J. Climate,* **23,** 4416–4428.

O'Gorman, P. A., 2011: The effective static stability experienced by eddies in a moist atmosphere. *J. Atmos. Sci.,* **68,** 75–90.

——, and T. Schneider, 2008a: Energy of midlatitude transient eddies in idealized simulations of changed climates. *J. Climate,* **21,** 3815–3832.

——, and ——, 2008b: The hydrological cycle over a wide range of climates simulated with an idealized GCM. *J. Climate,* **21,** 5797–5806.

——, and C. J. Muller, 2010: How closely do changes in surface and column water vapor follow Clausius–Clapeyron scaling in climate-change simulations? *Environ. Res. Lett.,* **5,** 025207, doi:10.1088/1748-9326/5/2/025207.

Pierrehumbert, R. T., 1995: Thermostats, radiator fins, and the local runaway greenhouse. *J. Atmos. Sci.,* **52,** 1784–1806.

Rowell, D. P., and R. G. Jones, 2006: Causes and uncertainty of future summer drying over Europe. *Climate Dyn.,* **27,** 281–299.

Schneider, T., and P. A. O'Gorman, 2008: Moist convection and the thermal stratification of the extratropical troposphere. *J. Atmos. Sci.,* **65,** 3571–3583.

——, ——, and X. J. Levine, 2010: Water vapor and the dynamics of climate changes. *Rev. Geophys.,* **48,** RG3001, doi:10.1029/2009RG000302.

Seneviratne, S. I., T. Corti, E. L. Davin, M. Hirschi, E. B. Jaeger, I. Lehner, B. Orlowsky, and A. J. Teuling, 2010: Investigating soil moisture–climate interactions in a changing climate: A review. *Earth Sci. Rev.,* **99,** 125–161.

Sobel, A. H., and C. S. Bretherton, 2000: Modeling tropical precipitation in a single column. *J. Climate,* **13,** 4378–4392.

Sutton, R. T., B. Dong, and J. M. Gregory, 2007: Land/sea warming ratio in response to climate change: IPCC AR4 model results and comparison with observations. *Geophys. Res. Lett.,* **34,** L02701, doi:10.1029/2006GL028164.

Troen, I. B., and L. Mahrt, 1986: A simple model of the atmospheric boundary layer; Sensitivity to surface evaporation. *Bound.-Layer Meteor.,* **37,** 129–148.